Si-Based Receivers for Optical Data Links

B. Jalali, *Member, IEEE*, L. Naval, *Member, IEEE*, and A. F. J. Levi

***Abstract*— We present results for Ge_xSi_{1-x} waveguide pin detectors grown by rapid thermal chemical vapor deposition (RTCVD). Detectors with multiple $Ge_{.29}Si_{.71}$ absorption layers show an internal quantum efficiency of 33% at $\lambda = 1.3$ μm with a dark current of 27 pA/μm^2. The external quantum efficiency is limited to 7% by the fiber-to-waveguide coupling efficiency. The output eye diagram for a hybrid $\lambda = 1.3$ μm silicon receiver at 500 Mb/s is demonstrated. Prospects of a silicon-based optoelectronic receiver array technology are discussed.**

I. Introduction

EXISTING electrical interconnection technologies pose a limitation to the performance of high-speed computation and switching systems. In future systems, it is likely that microprocessors operating at clock frequencies up to 1 GHz will be packaged with memory in a multichip module (MCM). Several MCM's will be mounted on a printed circuit board (PCB) and will have to communicate with other MCM's on other PCB's. Present technology allows for the possibility of a passive electrical bus supporting a 200 MHz clock frequency. It may be possible to use an active electrical bus to support clock frequencies up to 1 GHz, however, this is expensive to implement and thus susceptible to alternative technologies. The use of high-performance single channel and multiple channel array optical data links based on packaging of electronic and photonic devices is just such an alternative technology. A parallel optoelectronic data link may be the appropriate way to distribute a 32-b-wide digital bus with, for example, a composite bandwidth of $32 \times 0.5 = 16$ Gb/s. Some large computing and switching systems already take advantage of single channel optical data links in distributed computing architectures. However, the present cost of optical interconnection techniques limits their application to ultrahigh-performance or long distance transmission systems. Cost reduction is a critical factor to ensure an increasing market for optical data links. One way to achieve this is by use of the mature silicon technology in place of conventional III-V photonics. Although the realization of practical light emitting devices is impeded by the indirect energy bandgap of silicon, useful optical detection may be achieved. Also, the absorption coefficient can be extended to longer wavelengths by use of GeSi alloys. An all-silicon receiver in the wavelength range $\lambda = 0.8$ to 1.3 μm represents a cost reduction as well as enhancement in reliability compared to a conventional hybrid receiver consisting of a III-V pin photodetector and Si electronics.

Fig. 1 shows the absorption coefficient of Ge and Si versus wavelength. Also shown in the figure are the wavelengths for commercially available semiconductor lasers along with the loss and dispersion of glass fibers at these wavelengths. Both loss and dispersion are greater for shorter wavelengths. However, in short distance (≤ 1 km) transmission, the high power available from laser sources (compared to LED's) means that fiber loss is less important than the effect of fiber dispersion. Chromatic (intramode) dispersion limits the use of a system employing a Fabry–Perot laser with $\lambda = 0.8$ μm to less than 3 km for a 1 Gb/s nonreturn to zero (NRZ) digital signal. On the other hand, modal (intermode) dispersion imposes a bandwidth of 500 MHz/km for a typical multimode fiber which limits a 1 Gb/s point-to-point data link to lengths of less than 300 m. The use of $\lambda = 0.8$ μm wavelength would be desirable for two reasons: first, one can take advantage of low cost GaAs lasers (assuming they can meet the reliability requirement); second, the receiver may be implemented in pure silicon. The performance of such a system will be limited to communication lengths of a few hundred meters with data rates of less than 1 Gb/s. If synchronous parallel transmission is required, interconnect lengths are limited to 100 m by $\sigma = 3$ ps/m skew across a fiber array. Clearly, a "scalable" system which can be implemented over a wide range of communication length/bit rate is more desirable. In general, because of the 4% lattice mismatch between Si and Ge, the implementation of the receiver becomes more challenging at longer wavelength since the detector requires strained-layer epitaxial Ge_xSi_{1-x} films with higher Ge fraction. Consequently, one is inclined to conclude that a system operating at an intermediate range of, for example, $\lambda = 0.98$ μm or $\lambda = 1.3$ μm, provides a good compromise between the need for higher length/bit rate performance and the simplicity of its implementation GeSi pin detectors operating at $\lambda = 0.96$ μm have recently been reported [1]. In this paper, we present preliminary experimental results on Ge_xSi_{1-x} waveguide pin detectors operating at $\lambda = 1.3$ μm and grown by rapid thermal chemical vapor deposition (RTCVD). We further discuss the anticipated system performance based on these results.

II. Device Design

The low value of the absorption coefficient, caused by indirect bandgap of the alloy, can be overcome by making pin waveguide detectors in which light propagates normal to the direction of current flow [1]–[4]. This is made possible by the larger refractive index of Ge compared to Si which allows

Manuscript received June 23, 1993; revised January 18, 1994.

B. Jalali is with the Department of Electrical Engineering, University of California at Los Angeles, Los Angeles, CA 90024 USA.

L. Naval is with AT&T Bell Laboratories, 600 Mountain Ave., Murray Hill, NJ 07974 USA.

A. F. J. Levi is with the Department of Electrical Engineering and Electrophysics, University of Southern California, Los Angeles, CA 90089 USA.

IEEE Log Number 9400431.

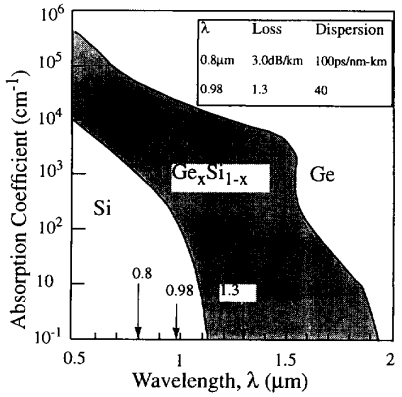

Fig. 1. Absorption coefficients of Ge and Si versus wavelength.

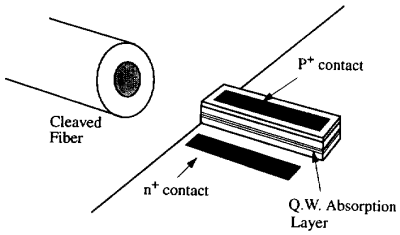

Fig. 2. Schematic of a waveguide pin detector.

fabrication of high-quality GeSi/Si waveguides [5], [6]. Fig. 2 shows the schematic of a waveguide pin photodetector. In such a structure, a thin (1–5 μm) intrinsic layer results in a short photocurrent transit delay, while device length may be kept long to compensate for the low absorption coefficient Because of lattice mismatch between Ge_xSi_{1-x} and the underlying Si, a multiple quantum well absorption layer is formed using thin layers of Ge_xSi_{1-x} sandwiched between Si barrier layers. The thickness of individual GeSi layers must be chosen to be below the equilibrium critical thickness [7]. The thickness of the Si barrier layers and the number of periods must ensure that the total thickness of the whole multiple quantum well layer is below the critical thickness corresponding to a layer with the average composition of the quantum well stack [8].

A typical device structure consists of a Ge_xSi_{1-x}/Si multiple quantum well absorption layer, Si cladding layers approximately 1 μm thick, and n^+ and p^+ contact layers. The resulting optically symmetric layer structure serve to improve the transverse optical confinement in the core layer. The external quantum efficiency of this detector is given by

$$\eta_{\text{ext}} = C(1-R)(1-e^{-\alpha_0 r \Gamma_T L}) \tag{1}$$

where R is the reflectivity of the waveguide front facet, C is the fiber-to-waveguide coupling efficiency, α_o is the bulk absorption coefficient of the Ge_xSi_{1-x} alloy (including the strain effects), ri s the quantum well duty cycle, L is the detector length, and Γ_T is the transverse optical confinement factor, which is given by [9]

$$\Gamma_T = \frac{\int_0^h |E(y)|^2\,dy}{\int_{-\infty}^{\infty} |E(y)|^2\,dy} \approx \frac{V^2}{2+V^2}. \tag{2}$$

In the above, y designates the transverse direction, and $E(y)$ is the transverse electric field distribution. The approximation is valid for the fundamental TE mode, with V being the normalized frequency and film thickness, defined as follows:

$$V = \frac{2\pi}{\lambda} h (n_{SL}^2 - n_s^2)^{1/2}. \tag{3}$$

Here, h is the thickness of the multiple quantum well core layer, n_{SL} is the average refractive index of the quantum well stack, and n_s is the refractive index for the substrate layer. Because of the large refractive index step between air and semiconductor in the lateral direction, we may assume that the lateral confinement factor, Γ_L, is close to unity.

III. Experiments

The devices are grown in a single wafer RAPRO rapid thermal chemical vapor deposition (RTCVD) system [1]. The system has a base pressure of 2×10^{-8} torr, and is equipped with a load-lock, an optical pyrometer, and a wafer rotation mechanism for achieving uniform growth rate across the wafer. Because growth rate and Ge incorporation must be carefully controlled, and also to maintain two-dimensional growth, the layers forming a GeSi/Si heterostructure are deposited at different temperatures. The rapid thermal technique is inherently suitable for growth of such structure with minimum interdiffusion and small processing time per wafer. Fig. 3 shows a typical layer structure for a pin diode consisting of a Ge_xSi_{1-x} multiple quantum well sandwiched between upper and lower intrinsic Si cladding layers and a $p = 1 \times 10^{19}$ cm^{-3} top contact layer. The structures are grown on (100) oriented n-type 4″ Czochralski substrates with an average resistivity of 0.018 Ω cm. GeSi layers are grown using SiH_2Cl_2 and GeH_4, and Si layers are grown using SiH_2Cl_2, both at a pressure of 4 torr. Wafer cleaning procedure consists of standard wet chemical clean followed by an in situ bake at 100°C for 1 min in a 50 torr H_2 ambient, GeSi alloys are grown in the temperature range 500°–590°C, depending on the Ge mole fraction. Films with higher Ge content must be grown at lower temperature in order to avoid three-dimensional island growth [10]. Furthermore, since the growth rate increases rapidly with increasing Ge content, substrate temperature must be reduced in order to maintain a low enough growth rate for thin films with a high percentage of Ge. In order to minimize the total growth time, Si layers are grown at a rate of 500 Å/min at an elevated temperature of 800°C.

The devices are fabricated in a standard silicon processing line used for fabrication of CMOS circuits. After growth, 5- and 10-μm-wide mesa structures are formed by reactive ion etching and passivation using deposited SiO_2. Windows are opened in the deposited oxide and a Ti/W-Al stack is used as ohmic contact metal. Fig. 4 shows an SEM photo of an 18-wide array of such devices with 250 μm spacing between devices. The intrinsic layer consists of 12 periods of $Ge_{.35}Si_{.65}$ (140 Å)/Si (500 Å), with 0.25 μm cladding layers.

These detectors exhibit sharp breakdown at approximately −40 V, with a variation of ±2 V across a 4″ wafer. The breakdown mechanism was investigated by measuring the breakdown voltage as a function of device temperature and

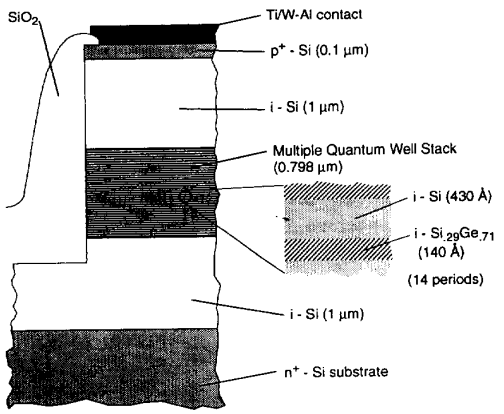

Fig. 3. Layer structure of a pin photodetector.

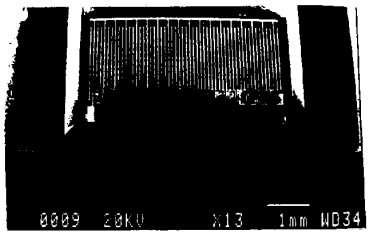

Fig. 4. SEM photograph of an 18-wide array of GeSi pin detectors.

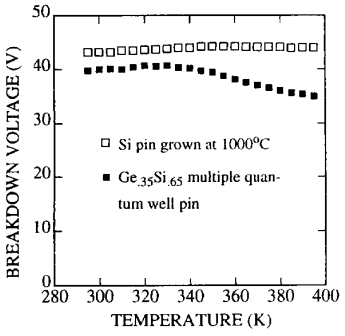

Fig. 5. Temperature dependence of breakdown voltage for GeSi quantum well pin diode shown in Fig. 4 and a device with Si intrinsic layer grown at 1000°C.

the results are shown in Fig. 5, where the breakdown voltage is measured at 1 μA. The figure shows the comparison of a device with multiple quantum well intrinsic layers and one with a silicon layer, or roughly the same thickness, which was grown at 1000°C. Comparison of breakdown values for the two different structures shows the high quality of low temperature epitaxial material.

Fig. 6 shows the measured external quantum efficiency η_{ext} for a device with the layer structure shown in Fig. 3. The device consists of 14 periods of $Ge_{.29}Si_{.71}$(140 Å)/Si(430 Å) multiple quantum well sandwiched between 1 μm intrinsic Si cladding layers on each side. The superlattice structures were

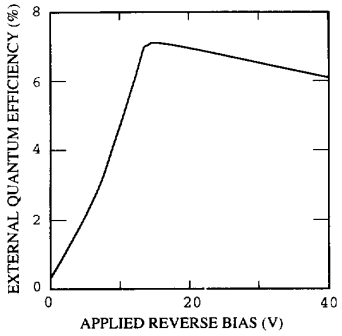

Fig. 6. External quantum efficiency versus applied bias measured for $\lambda = 1.32$ μm incident light.

characterized by a combination of Rutherford back scattering (RBS), giving the average composition, and transmission electron microscope (TEM), which shows the individual layer thickness. The thick cladding layers were grown in order to obtain a symmetric index profile and thus maximize the transverse optical confinement factor. Optical response measurements were obtained by butt coupling a single mode fiber with a 10 μm core diameter to a cleaved edge of the detector. The external quantum efficiency (for $\lambda = 1.32$ μm) increases with increasing reverse bias, reaching a maximum value of $\eta_{\text{ext}} = 7\%$ at $V_R = 14$ V. This behavior is possibly due to trapping of photo-excited carriers in the GeSi wells at low bias levels. These devices have an area of 10×750 μm^2 and a dark current of 27 pA/μm^2 at the bias corresponding to the peak quantum efficiency. The capacitance of the diodes was ~ 1 pF including the contributions from the metallization pads.

Fig. 7(a) shows the block diagram of a hybrid silicon-based receiver employing a GeSi waveguide pin packaged with a silicon bipolar transimpedance amplifier chip. The amplifier uses a 2 kΩ feedback resistor. Fig. 7(b) shows the receiver output eye-diagram for a 500 Mb/s NRZ pseudorandom $(2^7 - 1)$ optical input signal. The measured transimpedance of the amplifier at this speed is $Z = 64.9$ dB-Ω corresponding to a responsivity of 2.57 A W^{-1}. The receiver speed is limited by the transimpedance amplifier. This fact is confirmed in Fig. 8, which shows the detector eye-diagram at 1.5 Gb/s using a commercial 50 Ω GaAs amplifier with a bandwidth of 3 GHz. The rise and fall times in this case are approximately 110 ps. It should be noted that the eye-diagrams are degraded by the low input impedance of the amplifier. For reverse voltage of 14 V and greater, no trapping effects were observed in the transient measurements.

IV. Discussion

To gain insight into the factors determining the quantum efficiency, we must compare the experimentally measured external quantum efficiency, η_{ext}, to the theoretical value predicted by equation (1). This equation can be expressed as $\eta_{\text{ext}} = C(1 - R)\eta_{\text{int}}$, where $\eta_{\text{int}} = (1 - e^{-\alpha_o r \Gamma_T L})$ is the internal quantum efficiency.

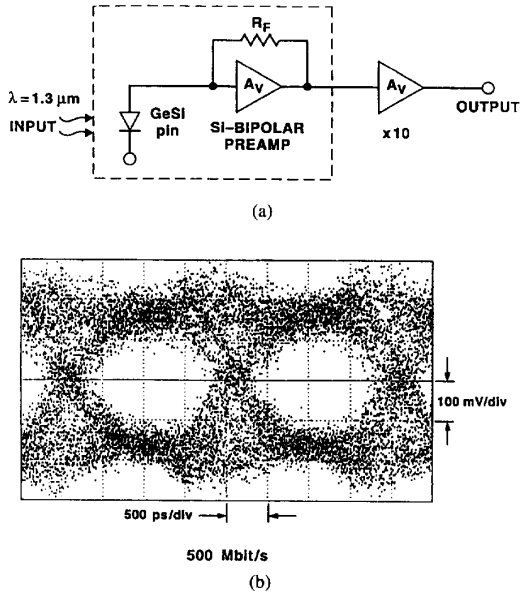

Fig. 7. (a) Block diagram and (b) output eye-diagram at 500 Mb/s for a hybrid silicon-based receiver at $\lambda = 1.3\ \mu m$.

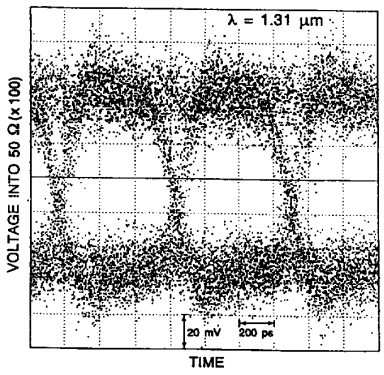

Fig. 8. Detector eye-diagram (×100) for a 1.5 Gb/s nonreturn-to-zero pseudorandom optical data stream.

The fiber-to-waveguide coupling efficiency, C, is given by the overlap integral of the waveguide and fiber near fields, namely,

$$C = \left[\int\int_{-\infty}^{\infty} E_g(x, y) \cdot E_f(x, y)\, dx\, dy\right]^2 \qquad (4)$$

where $E_g(x, y)$ and $E_f(x, y)$ are the normalized two-dimensional electric fields of the waveguide and the fiber, respectively. $E_g(x, y)$ is numerically calculated using the multilayer slab waveguide theory and the effective index method [11]. Fig. 9 shows the transverse (a) and contour (b) plots of the optical field intensity for the fundamental waveguide mode. $E_f(x, y)$ is obtained through analytical solution of the scalar wave equation. The refractive index for the GeSi alloy was obtained by a linear interpolation between $n_{Si} = 3.45$ and $n_{Ge} = 4.0$.

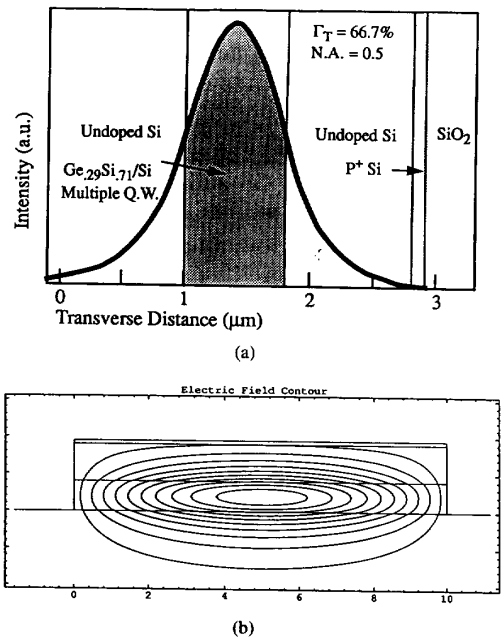

Fig. 9. Calculated (a) transverse and (b) contour plots of optical intensity for the fundamental mode.

For the $10 - \mu m$-wide step-index single mode fiber used in our experiments, we calculate $C = 0.3$. It should be noted that, with optimum fiber-guide positioning, the coupling efficiency is determined primarily by the overlap of the fiber field and that of the fundamental mode of the waveguide. Coupling into higher order modes is drastically reduced due to the mismatch between the polarization of fiber and waveguide fields. For normal incidence, the reflectivity of the front facet is $R = 0.3$, suggesting that $\eta_{int} = 33\%$. Further enhancement of the external quantum efficiency may be achieved by improving the internal efficiency. The latter can be obtained by optimizing the Ge content. In general, because of the constraints imposed by lattice mismatch, determination of the ideal material requires simultaneous optimization of the alloy absorption, the quantum well structure (accounting for quantum size effect) optical confinement in the core layer, and the fiber-to-waveguide coupling efficiency [12].

To assess the influence of dark current on performance of silicon-based optoelectronic integrated circuits (OEIC's), we consider its effect on the system sensitivity. The sensitivity of the receiver in a communication system is determined by the signal-to-noise ratio of front end detector and preamplifier. Because of the difference in bit rate (B) dependence of noise in bipolar transistors ($\sim B^2$) compared to field effect transistors ($\sim B^3$), bipolar front end amplifiers may be preferred for high-frequency (> 100 MB/s) operation [13]. As an example, we study bipolar transimpedance amplifiers using device parameters for a commercially available technology [14]. The sensitivity or the minimum detectable optical power, $\overline{P}$, for a receiver at $\lambda = 1.3\ \mu m$ is given by

$$\overline{P} = \frac{5.7}{\eta_{ext}}(\langle i^2\rangle_{cir} + \langle i^2\rangle_{pin})^{1/2} \qquad (5)$$

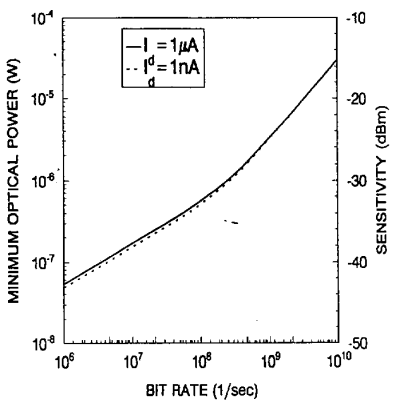

Fig. 10. Calculated sensitivity for a receiver front end consisting of a GeSi pin with $\eta_{ext} = 10\%$ and a bipolar transimpedance amplifiers.

where the first and second terms inside parentheses are the noise contributions from the circuit and the pin detector, respectively. Fig. 10 shows the calculated sensitivity of an optimized receiver consisting of a pin detector with $\eta_{ext} = 10\%$ and a bipolar transimpedance amplifier for a bit error rate of 10^{-9}. The solid and dashed lines correspond to detector dark currents of 1 μA and 1 nA, respectively. We note that even a dark current as high as 1 μA will have an insignificant effect on the receiver sensitivity. This reflects the fact that the front end amplifier noise is dominated by the thermal noise of the feedback resistor (2 kΩ, in this example) at low bit rates and by the collector current shot noise at high bit rates. Furthermore, with an external quantum efficiency of 10%, receiver sensitivities of -33 dBm at 100 Mb/s and -25 dBm at 1 Gb/s are possible in an optimized receiver.

We envision that silicon-based OEIC receivers will be used to form optoelectronic connector arrays. Fig. 11 shows a conceptual example of such a technology, in which accurate positioning of a multifiber array (up to 18 fibers) with respect to the silicon integrated optical receiver has been achieved by means of the AT&T MACII^{TM1} connector. The OEIC is mounted on the silicon submount with the optical-quality polished edges of the 18-photodetector array facing the fiber ends. The connector design allows convenient assembly and high fiber-to-guide optical intensity coupling. The OEIC electronic signals are wire-bounded to the submount microstrips available for that purpose.

V. Conclusion

We have discussed the prospects of Si-based receivers for optical data links GeSi waveguide pin detectors grown by RTCVD as well as an Si-based optical receiver operating at $\lambda = 1.3$ μm have been demonstrated. We expect that, with further improvements, silicon-based optoelectronic receiver technology will become a reality.

[1]TM MACH is a trademark of AT&T.

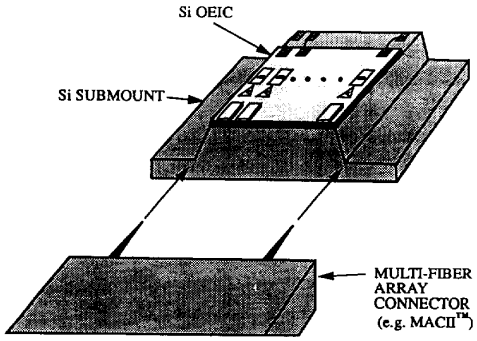

Fig. 11. Diagram of an Si-based integrated receiver mounted on an AT&T MACII^{TM} multifiber connector.

Acknowledgment

The authors would like to thank R. K. Montgomery and K. Ashby for providing the transimpedance amplifier, P. Watson and B. Weir for performing RBS and TEM measurements, and L. C. Feldman for helpful discussions and support.

References

[1] B. Jalali, A. F. J. Levi, F. Ross, and E. A. Fitzgerald, "SiGe waveguide photodetectors grown by rapid thermal chemical vapor deposition," *Electron. Lett.*, vol. 28, no. 3, pp. 269–271,1992.
[2] S. Luryi, T. P. Pearsall, H. Temkin, and J. C. Bean, "Waveguide infrared photodetectors on a silicon chip," *IEEE Electron Device Lett.*, vol. EDL-7, pp. 104–106,1986.
[3] T. P. Pearsall, H. Temkin, J. C. Bean, and S. Luryi, "Avalanche gain in Ge_xSi_{1-x} infrared waveguide detectors," *IEEE Electron Device Lett.*, vol. EDL-7, pp. 330–332, 1986.
[4] V. P. Kesan, G. V. Treyz, P. G. May, S. S. Iyer, and J. M. Halbout, "Integrated rib-waveguide Si/SiGe photodetector for long wavelengths," in *Proc. CLEO*, Baltimore, MD, May 13–17, 1991.
[5] R. A. Soref, F. Navamar, and J. P. Lorenzo, "Optical waveguiding in a single-crystal layer of germanium silicon grown on silicon," *Opt. Lett.*, vol. 15, no. 5, pp. 270–272, 1990.
[6] A. Splett, J. Schmidtchen, B. Schuppert,K. Pettermann, E. Kasper, and H. Kibbel, "Low loss optical ridge waveguides in a strained GeSi epitaxial layer grown on silicon," *Electron. Lett.*, vol. 26, no. 14, pp. 1035–1036, 1990.
[7] J. W. Matthews, and A. E. Blakeslee, "Defects in epitaxial multilayers," *J. Cryst. Growth*, vol. 27, pp. 118–125, 1974.
[8] R. Hull, J. C. Bean, F. Cerdeira, A. T. Fiory, and J. M. Gibson, "Stability of semiconductor strained-layer superlattices," *Appl. Phys. Lett.*, vol. 48, no. 1, pp. 56–58, 1986.
[9] G. P. Agrawal and N. K. Dutta, *Long-Wavelength Semiconductor Lasers*. New York: Van Nostrand Reinhold, 1986, p. 45.
[10] J. C. Bean, T. T. Sheng, L. C. Feldman, A. T. Fiory, and R. T. Lynch, "Pseudomorphic growth of Ge_xSi_{1-x} on silicon by molecular beam epitaxy," *Appl. Phys. Lett.*, vol. 44, no. 1, pp. 102–104, 1984.
[11] H. Kogelnik, "Theory of optical waveguides," in *Guided-Wave Optoelectronics*, 2nd ed., Springer Series in Electronics and Photonics, vol. 26, T. Tamir, Ed. Berlin: Springer-Verlag, 1990, pp. 43–50 and 69–74.
[12] L. Naval *et al.*, unpublished.
[13] R. G. Smith and S. D. Personick, "Receiver design for optical fiber communication systems," in *Topics in Applied Physics, vol. 39: Semiconductor Devices for Optical Communication*, H. Kressel, Ed. Heidelberg: Springer-Verlag, 1982, pp. 89–159.
[14] "CBIC-V Product Development Guide," AT&T Microelectronics, Dep. 52AL040420, 555 Union Blvd., Allentown, PA 18103.

B. Jalali (M'94), photograph and biography not available at the time of publication.

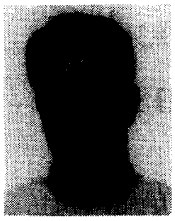

L. Naval (M'90) was born in Madrid, Spain, in 1964. He receiver the Ingeniero de Telecomunicación degree in microelectronics from the Universidad Politécnica de Madrid, Madrid, Spain, in 1989 in microelectronics.

After spending two years engaged in the development of CAD tools for VLSI design in AT&T Bell Laboratories (Allentown, PA, and Murray Hill, NJ), he started his research activity in optoelectronics in AT&T Bell Laboratories, Murray Hill, NJ, in 1991. He is currently pursuing the Ph.D. degree in electrical engineering. His present research interests include integrated optical guided-wave devices and silicon-based optoelectronics.

A. F. J. Levi, photograph and biography not available at the time of publication.